LUND UNIVERSITY

Multiple scattering by a collection of randomly located obstacles Part II: Numerical implementation - coherent fields

Gustavsson, Magnus; Kristensson, Gerhard; Wellander, Niklas

2014

Link to publication

Citation for published version (APA):
Gustavsson, M., Kristensson, G., & Wellander, N. (2014). *Multiple scattering by a collection of randomly located obstacles Part II: Numerical implementation - coherent fields*. (Technical Report LUTEDX/(TEAT-7236)/1-19/(2014); Vol. TEAT-7236). The Department of Electrical and Information Technology.

Total number of authors:
3

General rights
Unless other specific re-use rights are stated the following general rights apply:
Copyright and moral rights for the publications made accessible in the public portal are retained by the authors and/or other copyright owners and it is a condition of accessing publications that users recognise and abide by the legal requirements associated with these rights.
• Users may download and print one copy of any publication from the public portal for the purpose of private study or research.
• You may not further distribute the material or use it for any profit-making activity or commercial gain
• You may freely distribute the URL identifying the publication in the public portal

Read more about Creative commons licenses: https://creativecommons.org/licenses/

Take down policy
If you believe that this document breaches copyright please contact us providing details, and we will remove access to the work immediately and investigate your claim.

LUND UNIVERSITY

PO Box 117
221 00 Lund
+46 46-222 00 00

CODEN:LUTEDX/(TEAT-7236)/1-19/(2014)
Revision No. 1: January 2021

Multiple scattering by a collection of randomly located obstacles
Part II: Numerical implementation — coherent fields

Magnus Gustavsson, Gerhard Kristensson, and Niklas Wellander

Electromagnetic Theory
Department of Electrical and Information Technology
Lund University
Sweden

(TEAT-7236)/1-19/(2014): G. Kristensson, Multiple scattering by a collection of randomly located obstacles, Part II . . .

Magnus Gustavsson
Magnus.Gustafsson@foi.se

Swedish Defence Research Agency, FOI
P.O. Box 1165
SE-581 11 Linköping
Sweden

Gerhard Kristensson
Gerhard.Kristensson@eit.lth.se

Department of Electrical and Information Technology
Electromagnetic Theory
Lund University
P.O. Box 118
SE-221 00 Lund
Sweden

Niklas Wellander
Niklas.Wellander@foi.se

Swedish Defence Research Agency, FOI
P.O. Box 1165
SE-581 11 Linköping
Sweden

and

Department of Electrical and Information Technology
Electromagnetic Theory
Lund University
P.O. Box 118
SE-221 00 Lund
Sweden

Editor: Gerhard Kristensson
© M. Gustavsson, G. Kristensson, and N. Wellander, Lund, January 15, 2021

Abstract

A numerical implementation of a recently published rigorous theory that analyzes electromagnetic scattering by randomly located particles in a slab geometry is presented. In general, the particles can be of quite arbitrary shape, but, in this first implementation, all particles are identical dielectric spheres. The coherent part of the reflected and transmitted intensity at normal incidence is treated. An effective wave number of the slab is obtained from transmission data, and this value is compared with existing results in the literature with good agreement. Moreover, comparisons with the results of the Bouguer-Beer law (B-B) are made. The present theory also gives a small reflected coherent field, which is not predicted by the Bouguer-Beer law, and these results are discussed in some detail.

1 Introduction

Electromagnetic scattering by randomly located particles is frequently encountered in science. It is an important topic in terrestrial and atmospheric research, biomedical and life sciences, astrophysics, nanotechnology, just to mention a few. The literature is comprehensive, and we refer to the textbook literature and references therein, see *e.g.*, [9, 10, 21, 22, 27–30] for a survey of the field.

The literature contains several methods of computing the effective wave number, k_{eff}, for a half space containing a collection of randomly located spheres, see *e.g.*, [23–25,31,32] and [27, Chapter 6], and references therein. The effective wave number is obtained by solving a determinant relation and there are in general many solutions to this problem [6, 7]. The new method presented in Part I, [15, 16], does not suffer from these deficiencies and we are able to compute the coherent transmitted and reflected fields from a finite or an infinite slab containing randomly located scatterers. In this paper, we present transmission and reflection results for slabs with different thicknesses and spherical, non-magnetic particles (radius a) with relative permittivity $\epsilon_r = 1.33^2$. These data correspond to the permittivity of fresh water at optical frequencies. Both the electrical size of the spheres and the volume fraction are varied.

We organize the paper as follows: In Section 2 a brief introduction to the theory is presented. The numerical implementation is explained in Section 3 and the numerical results are presented in Section 4. We conclude the paper with a discussion in Section 5 and an appendix.

2 Theory

The theory of electromagnetic scattering by an ensemble of particles is reviewed in [9, 10, 19, 21, 22, 27–29].

The underlying theoretical treatment of the problem handled in this paper is presented in detail in Kristensson [15, 16]. The purpose of this section is to review

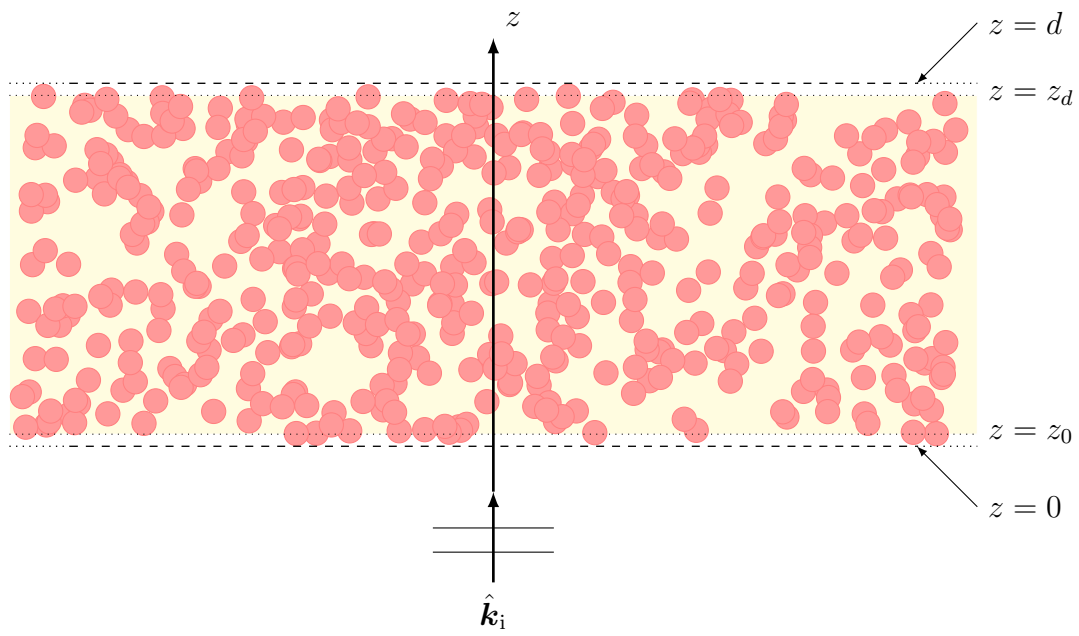

Figure 1: The geometry of the scattering region. The yellow region denotes the domain of possible locations of local origins, *i.e.*, the interval $[z_0, z_d] = [a, d - a]$.

and highlight some of the more important steps in the theory. For a more complete reference, we refer to Kristensson [15, 16].

We simplify the theoretical results in [15, 16] to a geometry of a slab ($z \in [0, d]$) and to spherical dielectric particles of radius a. These assumptions simplify the results considerably, and make the numerical implementation less demanding. The geometry is depicted in Figure 1. Notice that the domain of possible locations of local origins, $[z_0, z_d]$, is slightly smaller than the extent of the slab, *i.e.*, the interval is $[z_0, z_d] = [a, d - a]$, where a is the radius of the spheres.

Assume the incident field on the slab is[1]

$$\boldsymbol{E}_{\mathrm{i}}(z) = \boldsymbol{E}_0 \mathrm{e}^{\mathrm{i}k_0 z}$$

The coherent part (ensemble average) of the total electric field on either side of the slab is

$$\boxed{\langle \boldsymbol{E}(z) \rangle = \begin{cases} \boldsymbol{E}_{\mathrm{t}} \mathrm{e}^{\mathrm{i}k_0 z}, & z > d \\ \boldsymbol{E}_0 \mathrm{e}^{\mathrm{i}k_0 z} + \boldsymbol{E}_{\mathrm{r}} \mathrm{e}^{-\mathrm{i}k_0 z}, & z < 0 \end{cases}}$$

where the reflected and transmitted amplitudes, $\boldsymbol{E}_{\mathrm{t}}$ and $\boldsymbol{E}_{\mathrm{r}}$, respectively, are given

[1] Vectors are denoted in italic boldface, and matrices in roman boldface. A caret over a vector denotes a vector of unit length.

as[2]

$$\boldsymbol{E}_{\mathrm{t}} = \boldsymbol{E}_0 + \frac{3f}{4(k_0a)^3}\sum_{l=1}^{\infty}\mathrm{i}^{-l}\sqrt{\frac{2l+1}{2\pi}}\Bigg(\hat{\boldsymbol{x}}k_0\int_{z_0}^{z_d}\mathrm{e}^{-\mathrm{i}k_0z'}\left(f_{1\mathrm{o}1l}(z')+\mathrm{i}f_{2\mathrm{e}1l}(z')\right)\,\mathrm{d}z' - \hat{\boldsymbol{y}}k_0\int_{z_0}^{z_d}\mathrm{e}^{-\mathrm{i}k_0z'}\left(f_{1\mathrm{e}1l}(z')-\mathrm{i}f_{2\mathrm{o}1l}(z')\right)\,\mathrm{d}z'\Bigg) \tag{2.1}$$

and

$$\boldsymbol{E}_{\mathrm{r}} = \frac{3f}{4(k_0a)^3}\sum_{l=1}^{\infty}\mathrm{i}^{l}\sqrt{\frac{2l+1}{2\pi}}\Bigg(\hat{\boldsymbol{x}}k_0\int_{z_0}^{z_d}\mathrm{e}^{\mathrm{i}k_0z'}\left(f_{1\mathrm{o}1l}(z')-\mathrm{i}f_{2\mathrm{e}1l}(z')\right)\,\mathrm{d}z' - \hat{\boldsymbol{y}}k_0\int_{z_0}^{z_d}\mathrm{e}^{\mathrm{i}k_0z'}\left(f_{1\mathrm{e}1l}(z')+\mathrm{i}f_{2\mathrm{o}1l}(z')\right)\,\mathrm{d}z'\Bigg) \tag{2.2}$$

in terms of the volume fraction f of spheres, and the (unknown) coefficients $f_n(z)$. The coefficients $f_n(z)$ are the solution to a system of linear, one-dimensional integral equations in z, *viz.*,

$$\boxed{f_n(z) = \mathrm{e}^{\mathrm{i}k_0z}\sum_{n'}T_{nn'}a_{n'} + k_0\int_{z_0}^{z_d}\sum_{n'}K_{nn'}(z-z')f_{n'}(z')\,\mathrm{d}z', \quad z\in[z_0,z_d]} \tag{2.3}$$

where the transition matrix of the scatterers is denoted $T_{nn'}$, and where the explicit form of the kernel $K_{nn'}$ is ($\boldsymbol{r}_{\mathrm{c}} = x\hat{\boldsymbol{x}} + y\hat{\boldsymbol{y}}$) is

$$\boxed{K_{nn'}(z) = \frac{n_0}{k_0^3}\sum_{n''}T_{nn''}k_0^2\iint_{\mathbb{R}^2} g(|\boldsymbol{r}_{\mathrm{c}} - z\hat{\boldsymbol{z}}|)\mathcal{P}_{n''n'}(k_0(\boldsymbol{r}_{\mathrm{c}} - z\hat{\boldsymbol{z}}))\,\mathrm{d}x\,\mathrm{d}y}$$

Here, $g(r)$ is the pair distribution function [3, 20, 29, 34], and $\mathcal{P}_{nn'}(k_0\boldsymbol{d})$ is the translation matrix for the outgoing spherical vector waves [2]. The most simple pair distribution function models the hole correction (HC)

$$g(r) = H(r-2a) \tag{2.4}$$

where $H(x)$ is the Heaviside function and a is the radius of the spheres. The double integral in the definition of the kernel can be solved analytically for the hole correction in terms of a series of spherical waves [16, 17]. More complex distributions functions, *e.g.*, the hypernetted-chain equation, the Percus-Yevick approximation (P-YA), the self-consistent approximation, and Monte Carlo calculations are not employed in this paper [3, 20, 29, 34].

[2]In this paper, we adopt the multi-index notation $n = \tau\sigma ml$, where the integer indices $\tau = 1, 2$, $l = 1, 2, 3, \ldots$, $m = 0, 1, \ldots, l$, and $\sigma =$ e,o (even and odd in the azimuthal angle). In this paper, only $m = 1$ is employed, since the particles are spherical and the incidence is normal.

The particles are completely characterized by the transition matrix $T_{nn'}$, which for a spherical particle is diagonal in its (pairwise) indices, *i.e.*, $\delta_{nn'} = \delta_{\tau\tau'}\delta_{\sigma\sigma'}\delta_{mm'}\delta_{ll'}$. The coefficients a_n are the expansion coefficients of the incident plane wave in regular spherical vector waves. If the incident direction is along the positive z-direction, *i.e.*, $\hat{\boldsymbol{k}}_{\mathrm{i}} = \hat{\boldsymbol{z}}$, these are ($\sigma = \mathrm{e}$ is the upper line, and $\sigma = \mathrm{o}$ is the lower line)

$$\begin{cases} a_{1\sigma ml} = -\mathrm{i}^l \delta_{m1} \sqrt{2\pi(2l+1)} \left(\hat{\boldsymbol{z}} \times \begin{Bmatrix} \hat{\boldsymbol{x}} \\ \hat{\boldsymbol{y}} \end{Bmatrix} \right) \cdot \boldsymbol{E}_0 \\ a_{2\sigma ml} = -\mathrm{i}^{l+1} \delta_{m1} \sqrt{2\pi(2l+1)} \begin{Bmatrix} \hat{\boldsymbol{x}} \\ \hat{\boldsymbol{y}} \end{Bmatrix} \cdot \boldsymbol{E}_0 \end{cases} \qquad \hat{\boldsymbol{k}}_{\mathrm{i}} = \hat{\boldsymbol{z}}$$

where the vector $\boldsymbol{E}_0$ denotes the polarization state in the x-y plane.

The complex-valued transmission and reflection coefficients, t and r, that map the incident field to the transmitted and reflected fields, respectively, are defined by

$$\boxed{\boldsymbol{E}_{\mathrm{t}} = t\boldsymbol{E}_0, \qquad \boldsymbol{E}_{\mathrm{r}} = r\boldsymbol{E}_0} \tag{2.5}$$

The transmissivity T and the reflectivity R of the slab are given by

$$\boxed{T = \frac{|\boldsymbol{E}_{\mathrm{t}}|^2}{|\boldsymbol{E}_0|^2} = |t|^2, \qquad R = \frac{|\boldsymbol{E}_{\mathrm{r}}|^2}{|\boldsymbol{E}_0|^2} = |r|^2} \tag{2.6}$$

3 Numerical implementation

3.1 Numerical solution of the system of integral equations

To compute the reflection and the transmission coefficients of the slab, we need to solve (2.3) for given geometrical and material data. The equation is a linear system of Fredholm integral equations of the second kind [5], and we use the Nyström's method to solve the system of integral equations numerically [8, 14]. The unknown quantity, $f_n(z)$, is evaluated at set of quadrature points, $z = z_1, z_2, \ldots, z_p$, in the interval $[z_0, z_d]$, and the integral in (2.3) is evaluated by the use of the Simpson or Legendre quadrature rule at the points of discretization. The spatially discretized vector $f_n(z_p)$ is denoted $\boldsymbol{F}$. Remembering that n is a multi-index of $n = \{\tau\sigma ml\}$ ($m = 1$ in our application), the entries of the vector are organized as

$$\boldsymbol{F} = (f_{1\mathrm{e}11}(z_1) \cdots f_{1\mathrm{e}11}(z_p) \cdots f_{2\mathrm{o}1l_{\max}}(z_1) \cdots f_{2\mathrm{o}1l_{\max}}(z_p))^t \tag{3.1}$$

The discretized system has, in general, an overall linear dimension of $N = 4l_{\max}p$,[3] and the underlying integral equation in (2.3) is discretized as

$$\boxed{\boldsymbol{F} = \boldsymbol{P} + \mathbf{B} \cdot \boldsymbol{F} \quad \Leftrightarrow \quad (\mathbf{I} - \mathbf{B}) \cdot \boldsymbol{F} = \boldsymbol{P}}$$

[3]For a linearly polarized wave, the number of equations is reduced to $N = 2l_{\max}p$ for each Cartesian component, since there is no coupling between the set $\{\tau\sigma\} = \{1\mathrm{e}, 2\mathrm{o}\}$ and $\{\tau\sigma\} = \{1\mathrm{o}, 2\mathrm{e}\}$.

where $\mathbf{I}$ is the identity matrix, and the elements of matrix $\mathbf{B}$, $B_{nn'}$, are given by (3.2) below, which are the Simpson or Legendre quadrature weighted discretized kernel in (2.3) for n and n', respectively. The integration variable is discretized at the same points as the left-hand side and ordered the same way as the discrete vector $\boldsymbol{F}$. The form of the matrix $B_{nn'}$ is

$$\boxed{B_{nn'} = k_0 \begin{pmatrix} w_1 K_{nn'}(0) & w_2 K_{nn'}(z_1 - z_2) & \cdots & w_p K_{nn'}(z_1 - z_p) \\ w_1 K_{nn'}(z_2 - z_1) & w_2 K_{nn'}(0) & \cdots & w_p K_{nn'}(z_2 - z_p) \\ \vdots & \vdots & \ddots & \vdots \\ w_1 K_{nn'}(z_p - z_1) & w_2 K_{nn'}(z_p - z_2) & \cdots & w_p K_{nn'}(0) \end{pmatrix}} \tag{3.2}$$

where w_i, $i = 1, 2, \ldots, p$, are the ordinary Simpson or Legendre quadrature weights for numerical integration. The discretization of the single scattering contribution defines the vector $\boldsymbol{P}$ in the same format as $\boldsymbol{F}$, see (3.1), with vector elements given by

$$\boxed{P_n(z_i) = \mathrm{e}^{\mathrm{i}k_0 z_i} \sum_{n'} T_{nn'} a_{n'} \qquad i = 1, 2, \ldots, p}$$

We solve for the unknown vector $\boldsymbol{F}$ by the solution of a linear system of equations in MATLAB or Python 3.8, which also provides an implicit validation of the code. The transmitted and reflected fields are then found by using (2.1) and (2.2), respectively.

3.2 Computations of the effective wave number k_{eff}

Algorithm for determination of the effective wave number k_{eff}

We assume the spheres are non-magnetic, *i.e.*, $\mu_{\text{r}} = 1$.

1. Compute the transmission coefficient t with the method presented in Sections 2 and 3.1.

2. Compare the transmission coefficient t with the transmission coefficient t_{h} of a homogeneous slab of thickness d_{h} and wave number k. For a normally incident plane wave onto a non-magnetic slab, the transmission coefficient is [13]
$$t_{\text{h}}(k) = \frac{(1 - \Gamma_{\text{h}}^2) e^{\mathrm{i}(k - k_0) d_{\text{h}}}}{1 - \Gamma_{\text{h}}^2 e^{2\mathrm{i}k d_{\text{h}}}}$$
where $\Gamma_{\text{h}} = (k_0 - k)/(k_0 + k)$ and $k_0 = \omega/c_0$ is the wave number in vacuum.

3. Compute the effective wave number k_{eff} by finding the zeros of the function $G(k) = t - t_{\text{h}}(k)$, *i.e.*, the effective wave number, k_{eff}, satisfies $G(k_{\text{eff}}) = 0$.

The numerical algorithm for the determination of effective wave number k_{eff} of the slab, $z \in [0, d_{\text{h}}]$, is presented in the high-lighted note above. It differs from the traditional way of determining the effective wave number, which is done by solving for the roots of a determinant equation in the complex plane [27]. The effective wave number determined this way depends on the thickness of the slab, since the boundary effects are encapsulated in the algorithm.

To find the complex roots k_i of $G(k)$ in a given domain Ω in the complex plane, we employ either the secant method or the method described in Theorem A.1 in Appendix A (see also [18]). The secant method is fast and accurate, and the root finding algorithm is initialized by the effective wave number in the long wavelength (Rayleigh) limit, where the effective wave number is obtained by the Clausius-Mossotti's law [11] *viz.*,

$$\epsilon_{\text{eff}} = \frac{\epsilon_{\text{r}} + 2 + 2f(\epsilon_{\text{r}} - 1)}{\epsilon_{\text{r}} + 2 - f(\epsilon_{\text{r}} - 1)} = \begin{cases} 1.0061, & f = 0.01 \\ 1.0625, & f = 0.1 \end{cases}$$

$$k_{\text{eff}}/k_0 = \sqrt{\epsilon_{\text{r}}} = \begin{cases} 1.0031, & f = 0.01 \\ 1.0308, & f = 0.1 \end{cases}$$

With the latter method, the area Ω is subdivided into n sufficiently small rectangular domains, Ω_q, with boundaries γ_q. For each γ_q, the expression (A.1) is calculated using the midpoint rule. No initial value is needed with this method. If $k_i \in \Omega_q$, a test is made with a smaller contour to ensure that k_i is the single root inside γ_q. The process is repeated for every $\gamma_q \in \Omega$, and then for every frequency. Both methods give the same result. Among the available roots, the root closest to the solution at the previous frequency is chosen. For convenience, Ω was restricted to the region $0 \leq \operatorname{Im}\Omega \leq \sqrt{0.1}k_0$, $\sqrt{0.99}k_0 \leq \operatorname{Re}\Omega \leq \sqrt{2}k_0$ in our application.

In some of the figures below, see Figures 10, and 11, we compare the results of reflection and transmission with the corresponding results of a homogenized slab. With the particles confined within the slab $z \in [0, d]$, it is legitimate to ask what thickness the homogenized slab should have. The phase centers of the particles are located in the slab $[z_0, z_d] = [a, d - a]$, which differs from the confining slab by a diameter $2a$ of the particles. This issue is developed further in Section 4.4.

4 Results

In the numerical illustrations, we study the transmissivity and the reflectivity in (2.6) varying the thickness of the slab and the electrical size of the particles, which are assumed to be non-magnetic, $\mu_{\text{r}} = 1$, spheres with relative permittivity $\epsilon_{\text{r}} = 1.33^2$, corresponding to rain drops at optical frequencies. We also investigate how the volume fraction of scatters, f, affects the results. The parameters of the computations are summarized in Table 1.

The radiative transfer equation (RTE) is frequently used to infer the coherent and diffuse intensities of scattering by random particles in a slab geometry [9]. The coherent contribution in RTE is Bouguer-Beer law, which specifies the drop in the

Parameter	Value
ϵ_{r}	1.33^2
μ_{r}	1
d/a	$10, 50, 100$
$k_0 a$	$0 - 10$
f	$0.01, 0.1$

Table 1: Parameters of the numerical illustrations presented in this paper.

coherent intensity $I_{\mathrm{c}}(z)$, due to scattering and absorption in the material. The explicit form of the law is [9]

$$I_{\mathrm{c}}(z) = I_{\mathrm{c}}(0)\mathrm{e}^{-n_0 \sigma_{\mathrm{ext}} z} \tag{4.1}$$

where σ_{ext} is the single particle extinction cross section of the spheres [11], and the number density $n_0 = 3f/(4\pi a^3)$.

We also compare the method with the results of [27, Chapter 6]. This approach uses the same underlying theory — translations of spherical vector waves — to obtain a relation for the expansion coefficients of the scattered fields of the particles. A half-space geometry is employed and the expansion coefficients are assumed to have the form $A_n e^{\mathrm{i}k_{\mathrm{eff}} z}$. This leads to an infinite set of equations, and the effective wave number, k_{eff}, is found by a determinant relation. To generate results from [27, Chapter 6] a MATLAB code was downloaded from [26]. For comparison reasons, the Percus-Yevick pair distribution function was modified to the hole correction pair distribution function, see (2.4), by changing Equation (6.1.60) in [27, Chapter 6]. Even if the method in [27] and the one presented in this paper are based on the same underlying principles, the analysis diverges, and a comparison of the results is relevant. In addition, our method predicts the reflection properties of the slab as shown in Figures 10, and 11.

4.1 Computation parameters

The maximum number of terms included in the expansion is determined by the index l, which highest value is denoted l_{max}. The spatial discretization in the z variable is varied, depending on the slab thickness. The number of spatial discretization points, p, is increased until the variation of the result is sufficiently stable.The index m is fixed and takes the value $m = 1$, due to the excitation and the properties of the transition matrix of a spherical object. If we restrict the polarization of the incident field to the x axis, only $\{\tau\sigma\} = \{1\mathrm{o}, 2\mathrm{e}\}$ are engaged. This means that in practise the system (2.3) has $2l_{\mathrm{max}}p$ number of unknowns to be solved for.

4.2 Transmissivity as function of $k_0 a$

In Figures 2 and 3, we compare the transmissivity defined in (2.6) as a function of $k_0 a$ with the transmissivity computed with Bouguer-Beer law (B-B), (4.1), for

a slab with thickness $D/a = 98$, where $D = d - 2a$, consisting of non-magnetic dielectric spheres of radius a and $\epsilon_r = 1.33^2$. Two different volume fractions are used, $f = 0.01$ and $f = 0.1$. With B-B law, (4.1), the transmissivity is $T = I_c(D)/I_c(0)$, where $D = d - 2a$.[4] In Figure 2, we notice a very good agreement for $f = 0.01$ between the Bouguer-Beer law and the method presented in this paper. For $f = 0.1$ (Figure 3), the agreement is — in relative measures — less good, but good in absolute values, as both methods predict low transmissivity. For both volume fractions, the transmissivity has a global minimum in the studied frequency interval at $k_0 a \approx 6$. The increase in transmissivity at larger $k_0 a$ is due to the fact that the extinction cross section σ_{ext} decreases, see insert in Figure 3. This means that the spheres scatter less, and, hence, the coherent transmissivity increases.

There is a fine ripple in the transmissivity at low frequencies that is non-visible on the scale of the figure and hidden in the line thickness. This is illustrated in the insert in Figures 2 and 3. The effect diminishes at higher frequencies and the period of the ripple is different in the two figures (different volume fractions generate different effective wave numbers). The reason for this ripple is interference effects between the front and trailing end discontinuities in particle densities at $z = a$ and $z = d - a$. The period of the oscillation $\Delta(k_0 a)$ is

$$\Delta(k_0 a) = 2\pi \frac{k_0}{\operatorname{Re} k_{\text{eff}}} \frac{a}{2D} \tag{4.2}$$

where $D = d - 2a$. We discuss this ripple in more detail in Section 4.5 dealing with the reflectivity as a function of $k_0 a$.

In Figure 4 the real and imaginary part of transmission coefficient are plotted for $f = 0.01$ and $f = 0.1$ in the complex t plane with $k_0 a$ as a parameter along the curves. At higher volume fractions, the curve rapidly approaches the origin.

4.3 Transmissivity as function of volume fraction f

In Figure 5, the transmissivity T is plotted as a function of the volume fraction f at $k_0 a = 10$. We note good agreement between our method and Bouguer-Beer law for small f, but at higher volume fractions the curves start to deviate. A possible explanation to the discrepancies between the Bouguer-Beer law and the present method at higher volume fractions is that the far field criterion is assumed between the scatterers in the Bouguer-Beer law. At lower concentrations, this assumptions is more accurate, hence the Bouguer-Beer law and our method agree more. Moreover, no boundary effects are included in the Bouguer-Beer law.

4.4 Computations of the effective wave number k_{eff}

The effective wave number, k_{eff}, is calculated using the transmission coefficient of the coherent field, as described in Section 3.2, for different slab-thicknesses d. For

[4] Notice that the thickness of the slab is $D = d - 2a$. There is a slight difference between the geometrical thickness d of the containing slab (thickness of the material), and the quantity $D = d - 2a$, which measures the thickness of the scatterer's phase centers in the slab, see also in Section 4.5 below.

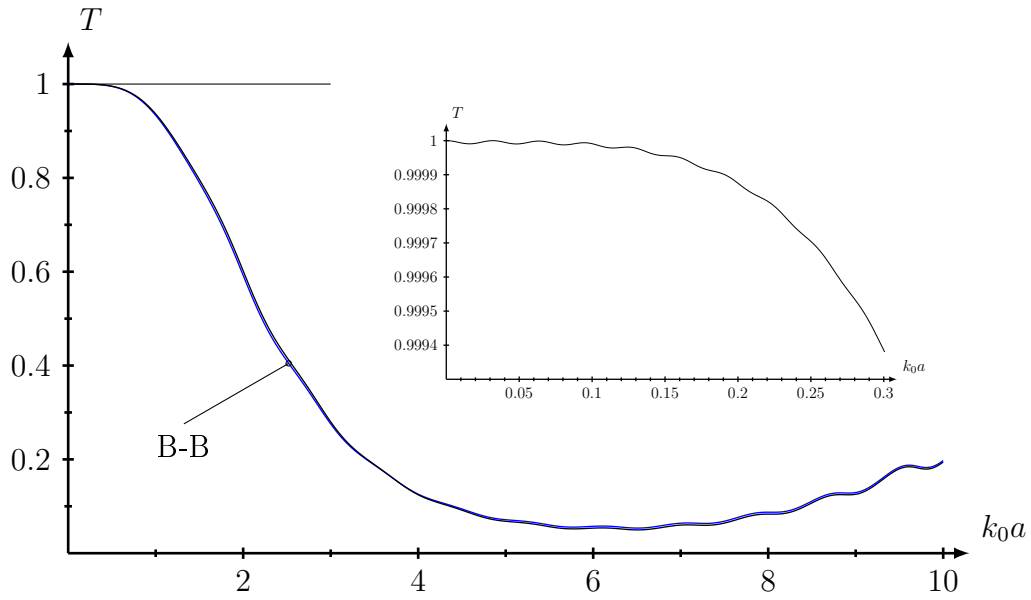

Figure 2: The transmissivity T (coherent part) as a function of the electrical size k_0a for a slab thickness of $d/a = 100$ and constant volume fraction $f = 0.01$. The blue line is the result obtained by the Bouguer-Beer law (B-B). The insert shows the fine ripple that occurs at low frequencies.

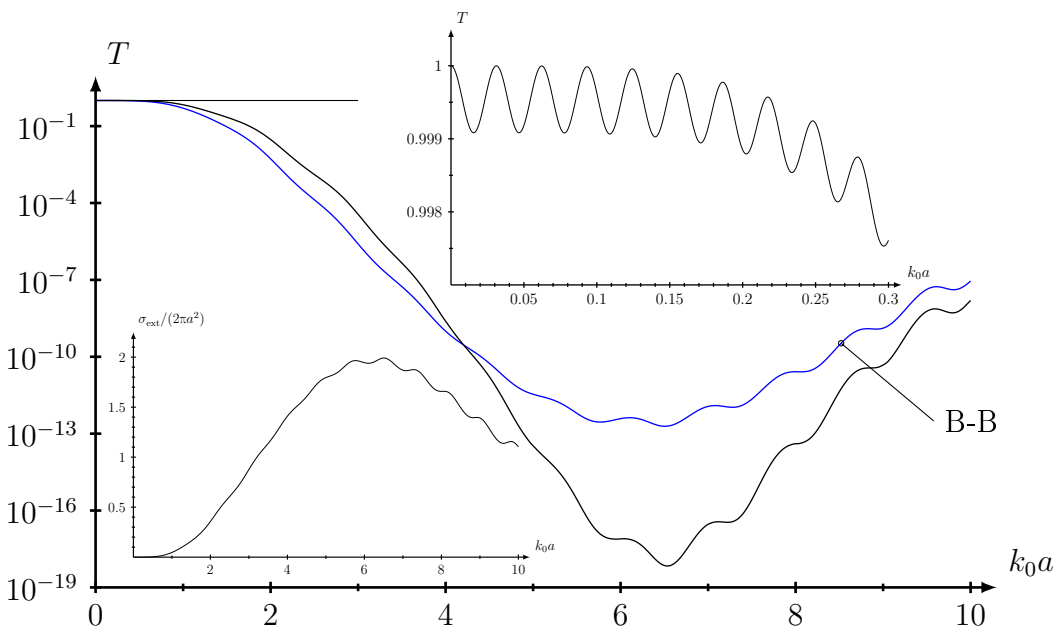

Figure 3: The same data as in Figure 2, but with $f = 0.1$ and in log-scale on the vertical axis. The insert to the left shows the extinction cross section $\sigma_{\text{ext}}/(2\pi a^2)$ for a single sphere as a function of the frequency k_a. Notice that minimum transmission coincides with the maximum in the extinction cross section.

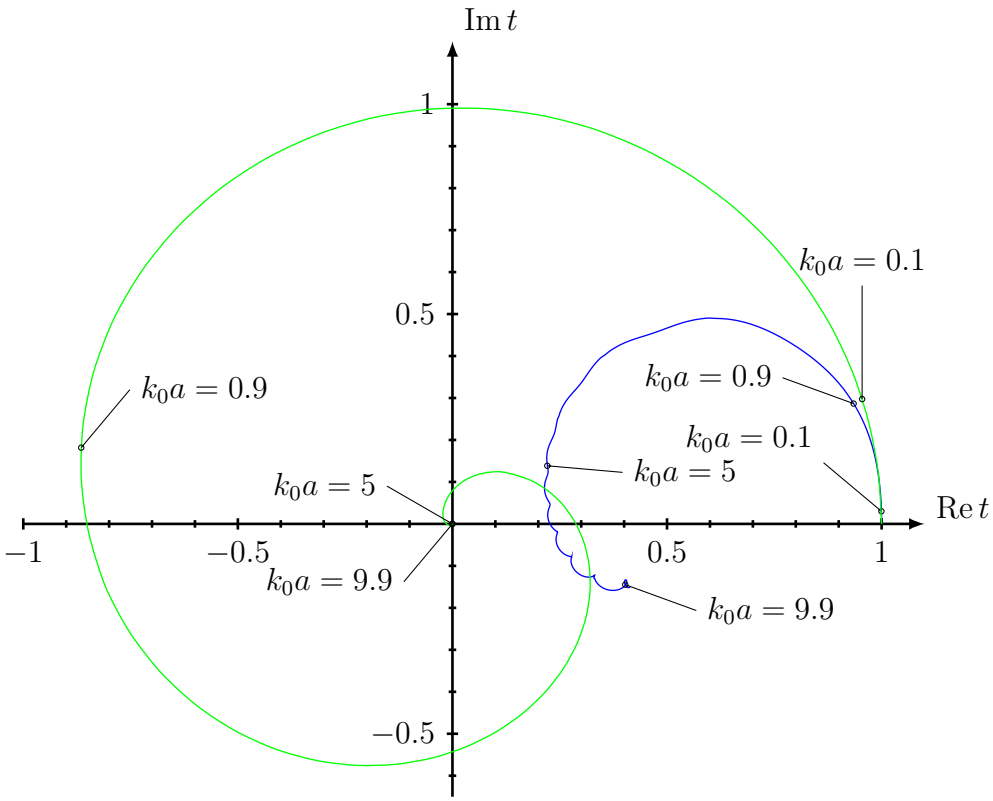

Figure 4: The components of the complex-valued transmission coefficient, $t(k_0a)$, in the complex plane as a function of the electrical size k_0a for a slab of thickness $d/a = 100$ and constant volume fraction $f = 0.01$ (blue curve) and $f = 0.1$ (green curve).

each choice of d, the algorithm in the high-lighted note in Section 3.2 determines a set of effective wave numbers that match the transmission data. It is, however, not obvious what slab thickness to use in this algorithm. Specifically, the geometrical extent of the containing slab is d, and the extent of the phase centers is $D = d - 2a$. In the discussion above in Section 4.2, we found that using a thickness D gave consistent periodicity of the fine ripple at low frequencies for the reflection data. This observation validates that the electrical thickness of the slab is D (also supported by the integration interval in the system of integral equations in (2.3)), and in this paper we use this value in our computations as the thickness of the homogenized slab.

In Figures 6 and 7, we compare the results of [27] and the results presented in this paper of determining the effective wavenumber k_{eff}. The wave number k_{eff} is normalized with the wave number of vacuum, k_0. The result computed with the method in [27] originates from a half-space. We notice that the values of k_{eff} computed with the present method for both $d_{\text{h}}/a = 10, 50, 100$ and $d_{\text{h}}/a = 8, 48, 98$ and the results given in [27] differ. The differences get smaller as the slab gets wider, and the values $d_{\text{h}}/a = 8, 48, 98$ have a better fit, which further supports the fact

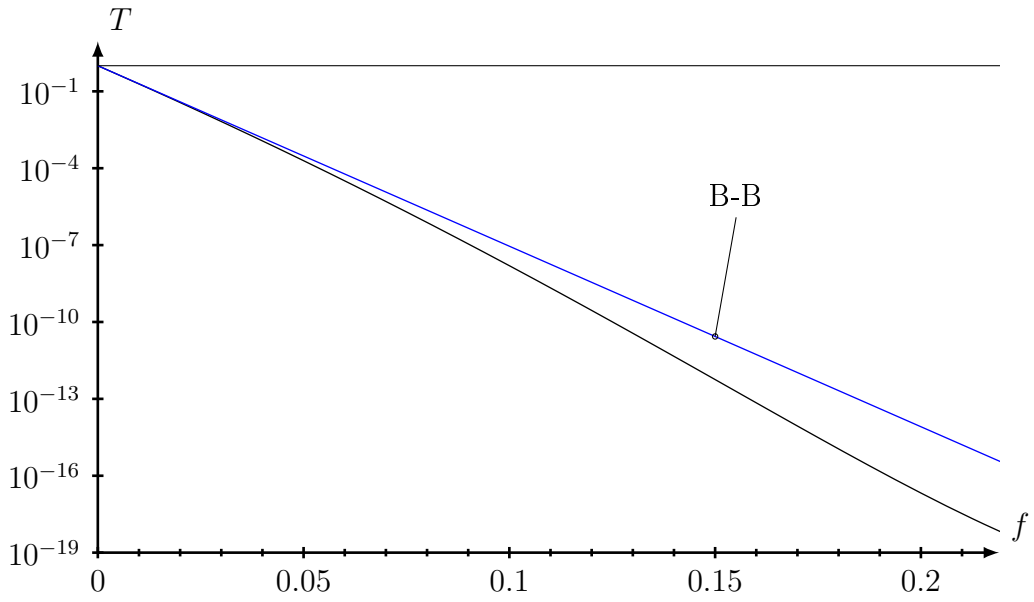

Figure 5: The transmissivity T (coherent part) in log scale as a function of the volume fraction f for a slab of thickness $d/a = 100$ and constant electrical size $k_0 a = 10$. The blue line is the result obtained by the Bouguer-Beer law (B-B).

that the thickness of the electrical thickness is D.

4.5 Reflectivity as function of $k_0 a$

The reflection coefficient for a homogeneous slab of thickness d_{h} and wave number k is given by [13]

$$r_{\mathrm{h}}(k) = \Gamma_{\mathrm{h}} \frac{1 - e^{2\mathrm{i}kd_{\mathrm{h}}}}{1 - \Gamma_{\mathrm{h}}^2 e^{2\mathrm{i}kd_{\mathrm{h}}}} \tag{4.3}$$

where Γ_{h} is given in the high-lighted note in Section 3.2.

The reflectivity R as a function of the frequency parameter $k_0 a$ for $d/a = 100$ and volume fractions $f = 0.01, 0.1$ is shown in Figures 8 and 9, respectively. The low-frequency ripple is clearly shown in these figures, and the period of the ripple depends of the volume fraction f as well as the thickness D, see (4.2). The figures also contain a comparison of the reflectivity with a homogenized slab using the effective wave number computed in Section 4.4 (see Figures 6 and 7). The effective wave number k_{eff} depends on the parameters f and D.

Notice that the period of the blue curves overlap the correct reflectivity (black curves). This is an indirect proof that $D = d - 2a$ is the electric thickness of the slab filled with particles. This is also supported by the integration interval in the system of integral equations (2.3), and the period of the ripple supports that the period is related to the length scale $2D$. The reflectivity of the homogenized slab agrees well for low frequencies, and deviates at higher frequencies. In contrast to the transmissivity, the ripple in the reflectivity extends to higher frequencies.

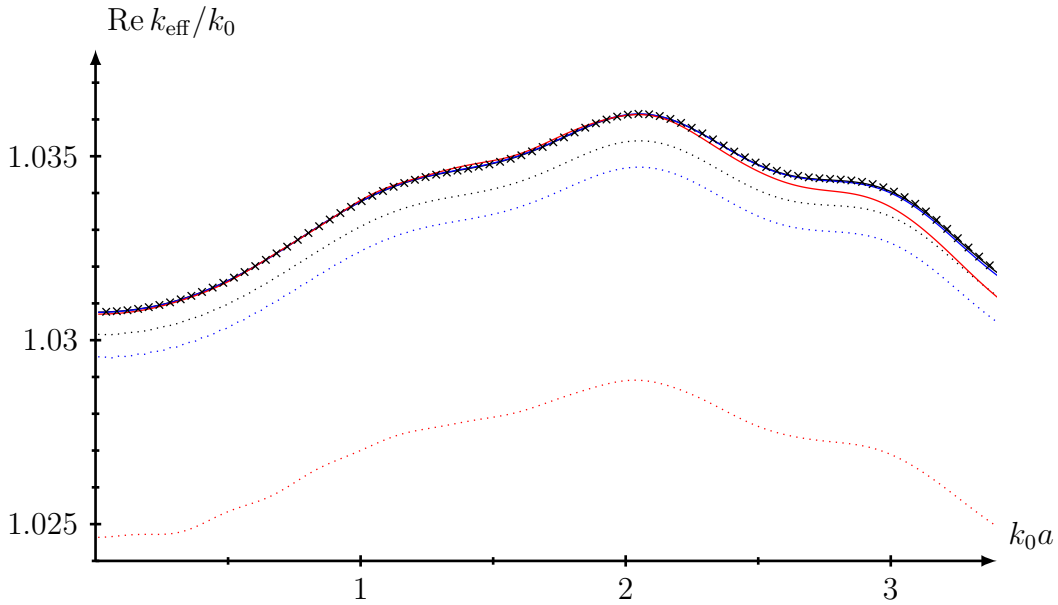

Figure 6: The real component of the scaled effective wave number, k_{eff}/k_0, as a function of the electrical size k_0a for a slab of thickness $d_{\text{h}}/a = 8, 48, 98$ (red, blue, and black solid curves, respectively) and $d_{\text{h}}/a = 10, 50, 100$ (red, blue and, black dotted curves, respectively) and constant volume fraction $f = 0.1$. The crosses are the result by [27].

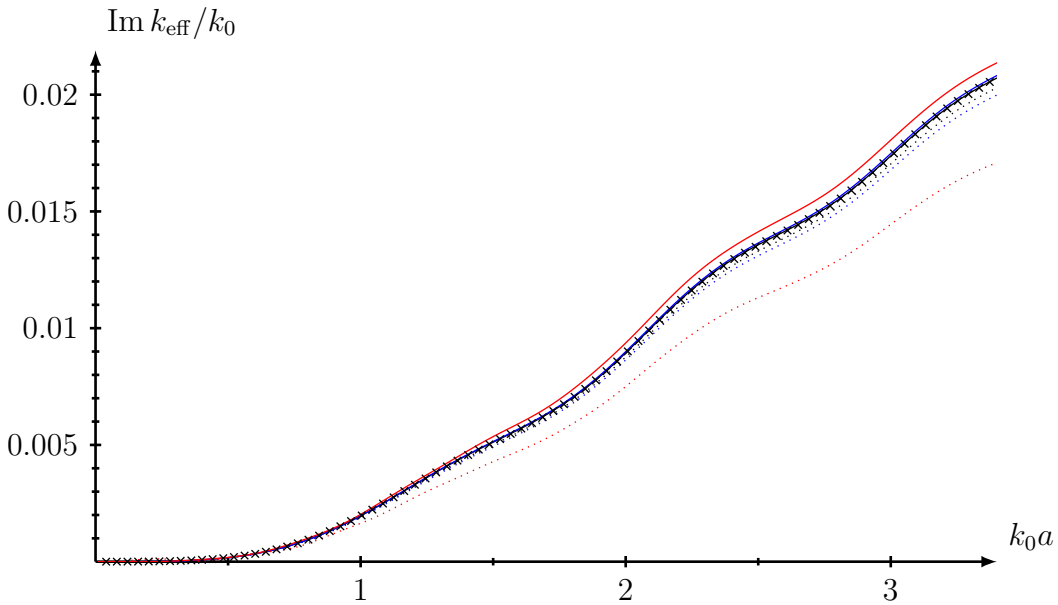

Figure 7: The imaginary component of the scaled effective wave number, k_{eff}/k_0, as a function of the electrical size k_0a. Data are identical to the ones in Figure 6.

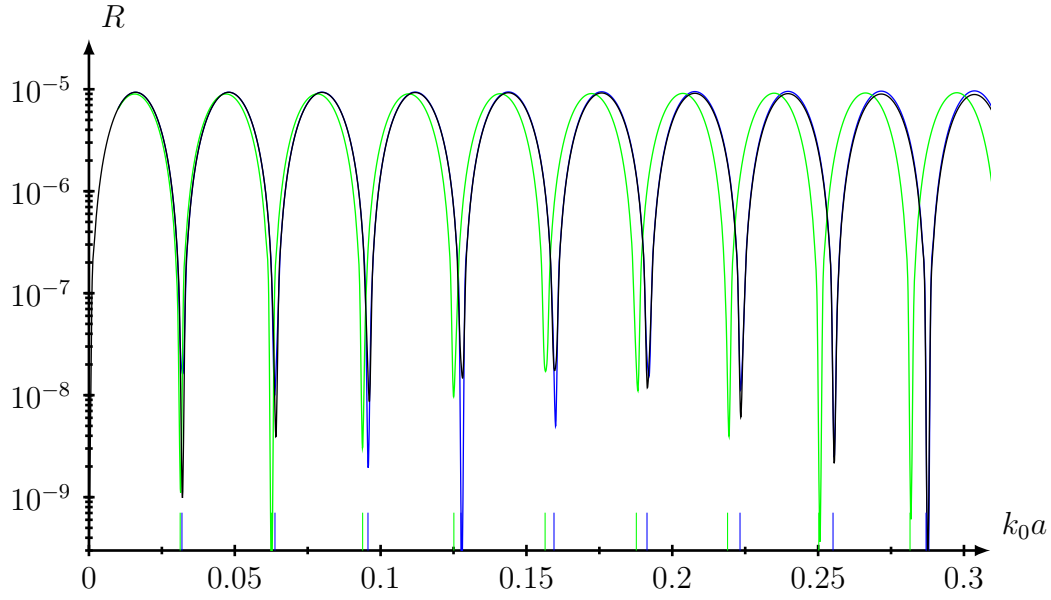

Figure 8: The reflectivity R (coherent part) in log scale as a function of the electrical size k_0a (black curve). The slab thickness is $d/a = 100$ and the volume fraction $f = 0.01$. The blue and green curves show the reflectivity from an homogeneous slab with effective wave number for $f = 0.01$ and slab thickness $d_{\mathrm{h}}/a = 98, 100$, respectively. The blue and green vertical lines show the periods $\pi/1.0031/98$ and $\pi/1.0031/100$, respectively.

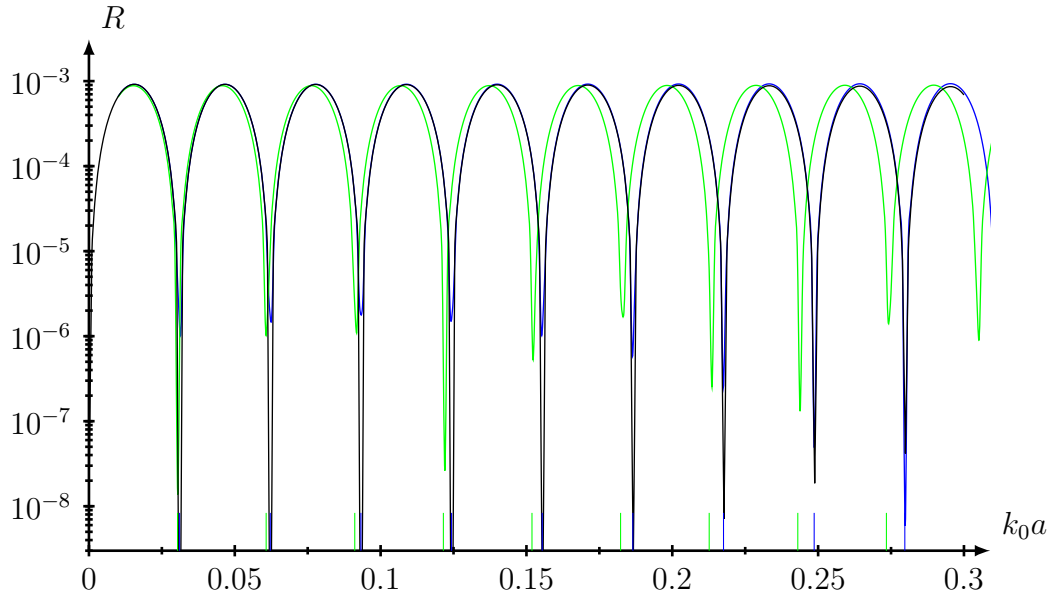

Figure 9: The same as in Figure 8, but with $f = 0.1$. The reflectivity from the homogenized slabs uses the effective wave number from Figures 6 and 7. The blue and green vertical lines show the periods $\pi/1.0308/98$ and $\pi/1.0308/100$, respectively.

In Figures 10 and 11, we show the reflectivity, R, see (2.6), for a volume fraction $f = 0.01$, with containing slab thickness $d/a = 10, 50$, respectively. The thickness of the homogenized slab is $d_{\mathrm{h}}/a = D/a = 8, 48$, respectively. As the ripple mention above is present, it is difficult to make an illustration over the entire frequency interval $k_a \in [0, 10]$, because the many oscillations obstruct the curve. However, in Figure 12 we depict the reflectivity over a larger frequency interval, but for a denser and thicker particulate material ($d/a = 50$, $f = 0.1$).

The results shown in Figures 10 and 11 are compared with the reflectivity, computed with (4.3) with effective wave number k_{eff} obtained with the algorithm in the high-lighted note in Section 3.2. These figures show the reflectivity for a thinner slab than the ones in Figures 8 and 9. We obtain good agreement between the two ways of computing reflection data for small $k_0 a$. This means that k_{eff} is a solution to both $G(k) = 0$, see Section 3.2 for definition, and $r - r_{\mathrm{h}}(k) \approx 0$ when $k_0 a$ is small, where r is computed by (2.5) and $r_{\mathrm{h}}(k)$ is given in (4.3). For these parameter values, when the wavelength of the electromagnetic field is large compared with the size of the particles, classical homogenization methods hold (*e.g.*, see [1, 4, 12, 33]).

5 Discussion and conclusions

We have presented numerical results for the method described in [16] to model the coherent reflected and transmitted fields for a slab of finite thickness containing randomly distributed spherical particles of equal size and relative permittivity, ϵ_{r}. The wave number for the transmitted field agrees well with the effective wave number obtained by the method given in [27, Chapter 6] if the thickness of the slab is large.

We have observed that the reflection by the slab is consistent with the reflection by a homogeneous slab at low frequencies and verifies that homogenization methods are useful.

We have used the hole correction, which is applicable for *e.g.*, gases. In the future, another type of hole correction should be implemented. Extensions to oblique incidence are also planned.

Appendix A Zeros and poles of an analytic function

The determination of the location of zeros of an analytic function is vital in the computations of the effective wave number in this paper. The following theorem is then useful [18]:

Theorem A.1. *Let Ω be an open domain in the complex z-plane, and let $f(z)$ be an analytic function in Ω with a simple zero at z_0. Then*

$$z_0 = \frac{\displaystyle\oint_\gamma \frac{z \, \mathrm{d}z}{f(z)}}{\displaystyle\oint_\gamma \frac{\mathrm{d}z}{f(z)}}$$

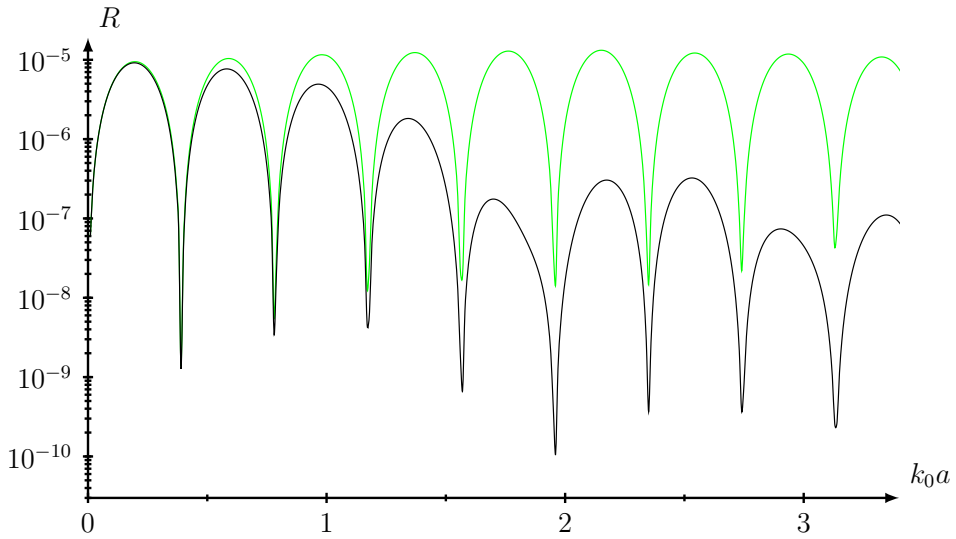

Figure 10: Reflectivity R (coherent part) v.s. frequency in log scale for a slab of thickness $d/a = 10$ and constant volume fraction $f = 0.01$. The green line is the result obtained by reflection by a homogeneous slab.

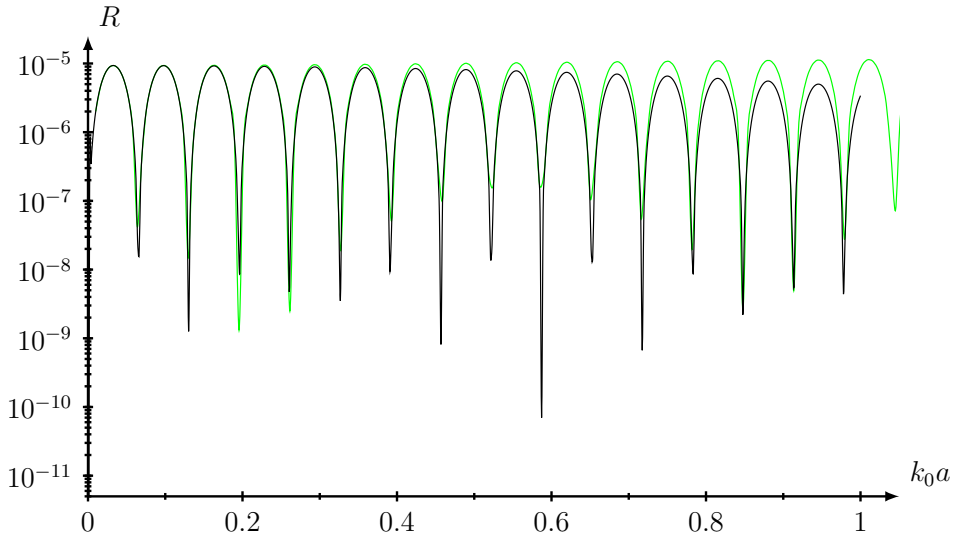

Figure 11: Reflectivity R (coherent part) v.s. frequency in log scale for a slab of thickness $d/a = 50$ and constant volume fraction $f = 0.01$. The green line is the result obtained by reflection by a homogeneous slab.

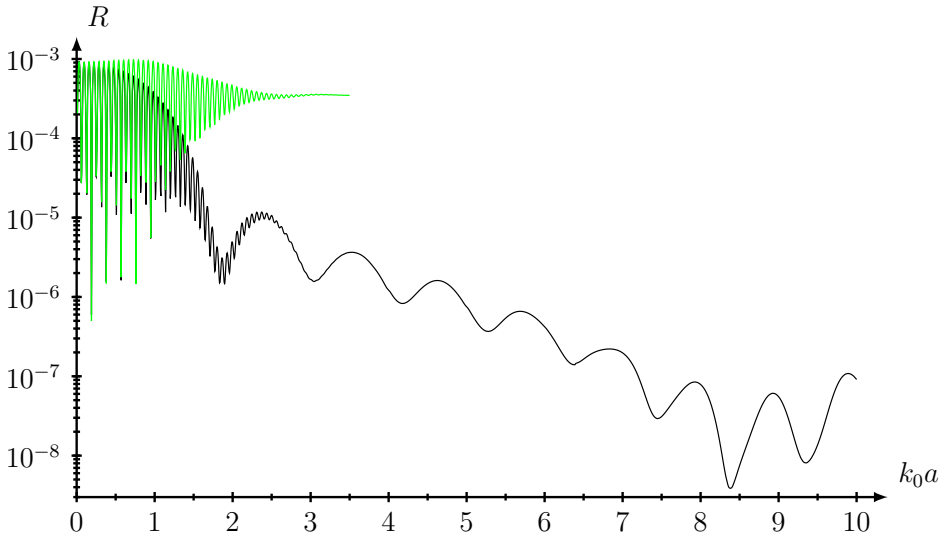

Figure 12: Reflectivity R (coherent part) v.s. frequency in log scale for a slab of thickness $d/a = 50$ and constant volume fraction $f = 0.1$. Noticed that the ripple at low frequencies vanishes at higher frequencies. The green line is the result obtained by reflection by a homogeneous slab.

where γ is any contour that lies inside Ω, and that encircles the zero z_0.

We give the proof of this theorem.

Proof. Since the zero is simple the function $f(z)$ is

$$f(z) = g(z)(z - z_0), \quad z \in \Omega$$

where $g(z)$ has no zeroes in Ω. The residue theorem then gives

$$\oint_\gamma \frac{z\,\mathrm{d}z}{f(z)} = 2\pi\mathrm{i}\,\mathrm{Res}\,\frac{z}{f(z)}\bigg|_{z=z_0} = 2\pi\mathrm{i}\frac{z_0}{g(z_0)}$$

Similarly,

$$\oint_\gamma \frac{\mathrm{d}z}{f(z)} = 2\pi\mathrm{i}\frac{1}{g(z_0)}$$

and the theorem is proved. □

References

[1] A. Bensoussan, J. L. Lions, and G. Papanicolaou. *Asymptotic Analysis for Periodic Structures*, volume 5 of *Studies in Mathematics and its Applications*. North-Holland, Amsterdam, 1978.

[2] A. Boström, G. Kristensson, and S. Ström. Transformation properties of plane, spherical and cylindrical scalar and vector wave functions. In V. V. Varadan, A. Lakhtakia, and V. K. Varadan, editors, *Field Representations and Introduction to Scattering*, Acoustic, Electromagnetic and Elastic Wave Scattering, chapter 4, pages 165–210. Elsevier Science Publishers, Amsterdam, 1991.

[3] V. Bringi and V. Varadan. The effects on pair correlation function of coherent wave attenuation in discrete random media. *Antennas and Propagation, IEEE Transactions on*, **30**(4), 805–808, 1982.

[4] D. Cioranescu and P. Donato. *An introduction to homogenization*, volume 17 of *Oxford Lecture Series in Mathematics and its Applications*. Oxford University Press, Oxford, 1999.

[5] L. M. Delves and J. L. Mohamed. *Computational methods for integral equations*. CUP Archive, 1988.

[6] A. L. Gower, I. D. Abrahams, and W. J. Parnell. A proof that multiple waves propagate in ensemble-averaged particulate materials. *Proc. R. Soc. A*, **475**(2229), 20190344, 2019.

[7] A. L. Gower, W. J. Parnell, and I. D. Abrahams. Multiple waves propagate in random particulate materials. *SIAM J. Appl. Math.*, **79**(6), 2569–2592, 2019.

[8] W. Hackbusch. *Integral Equations, Theory and Numerical Treatment*. Birkhäuser, Basel, 1995.

[9] A. Ishimaru. *Wave propagation and scattering in random media. Volume 1. Single scattering and transport theory*. Academic Press, New York, NY, 1978.

[10] A. Ishimaru. *Wave propagation and scattering in random media. Volume 2. Multiple scattering, turbulence, rough surfaces, and remote sensing*. Academic Press, New York, NY, 1978.

[11] J. D. Jackson. *Classical Electrodynamics*. John Wiley & Sons, New York, NY, third edition, 1999.

[12] V. V. Jikov, S. M. Kozlov, and O. A. Oleinik. *Homogenization of Differential Operators and Integral Functionals*. Springer-Verlag, Berlin, 1994.

[13] J. A. Kong. *Electromagnetic Wave Theory*. John Wiley & Sons, New York, NY, 1986.

[14] R. Kress. *Linear Integral Equations*. Springer-Verlag, Berlin Heidelberg, second edition, 1999.

[15] G. Kristensson. Multiple scattering by a collection of randomly located obstacles. Part I: Theory — coherent fields. Technical Report LUTEDX/(TEAT-7235)/1–49/(2014), Lund University, Department of Electrical and Information Technology, P.O. Box 118, S-221 00 Lund, Sweden, 2014.

[16] G. Kristensson. Coherent scattering by a collection of randomly located obstacles — an alternative integral equation formulation. *J. Quant. Spectrosc. Radiat. Transfer*, **164**, 97–108, 2015.

[17] G. Kristensson. Evaluation of some integrals relevant to multiple scattering by randomly distributed obstacles. *Journal of Mathematical Analysis and Applications*, **432**(1), 324–337, 2015.

[18] G. Kristensson. *Scattering of Electromagnetic Waves by Obstacles.* Mario Boella Series on Electromagnetism in Information and Communication. SciTech Publishing, Edison, NJ, USA, 2016.

[19] P. A. Martin. *Multiple Scattering: Interaction of Time-Harmonic Waves with N Obstacles*, volume 107 of *Encyclopedia of Mathematics and its Applications.* Cambridge University Press, Cambridge, 2006.

[20] D. A. McQuarrie. *Statistical mechanics.* University Science, Sausalito, USA, 2000.

[21] M. I. Mishchenko. *Electromagnetic Scattering by Particles and Particle Groups. An Introduction.* Cambridge University Press, New York, NY, 2014.

[22] M. I. Mishchenko, L. D. Travis, and A. A. Lacis. *Multiple scattering of light by particles: radiative transfer and coherent backscattering.* Cambridge University Press, Cambridge, 2006.

[23] V. P. Tishkovets. Multiple scattering of light by a layer of discrete random medium: backscattering. *J. Quant. Spectrosc. Radiat. Transfer*, **72**(2), 123–137, 2002.

[24] V. P. Tishkovets and M. I. Mishchenko. Coherent backscattering of light by a layer of discrete random medium. *J. Quant. Spectrosc. Radiat. Transfer*, **86**(2), 161–180, 2004.

[25] V. Tishkovets, E. Petrova, and M. Mishchenko. Scattering of electromagnetic waves by ensembles of particles and discrete random media. *J. Quant. Spectrosc. Radiat. Transfer*, **112**, 2095–2127, 2011.

[26] L. Tsang and J. Kong. Electromagnetic Wave MATLAB Library, 2006. http://www.ee.washington.edu/research/laceo/emwave.

[27] L. Tsang and J. A. Kong. *Scattering of Electromagnetic Waves: Advanced Topics.* John Wiley & Sons, New York, NY, 2001.

[28] L. Tsang, J. A. Kong, and K.-H. Ding. *Scattering of Electromagnetic Waves: Theories and Applications.* John Wiley & Sons, New York, NY, 2000.

[29] L. Tsang, J. A. Kong, K.-H. Ding, and C. O. Ao. *Scattering of Electromagnetic Waves: Numerical Simulations.* John Wiley & Sons, New York, NY, 2001.

[30] K. K. Tse, L. Tsang, C. H. Chan, and K.-H. Ding. Multiple scattering of waves by random distribution of particles for applications in light scattering by metal nanoparticles. In *Light Scattering and Nanoscale Surface Roughness*, pages 341–370. Springer, 2007.

[31] V. K. Varadan, V. N. Bringi, and V. V. Varadan. Coherent electromagnetic wave propagation through randomly distributed dielectric scatterers. *Phys. Rev. D*, **19**(8), 2480–2489, April 1979.

[32] V. V. Varadan and V. K. Varadan. Multiple scattering of electromagnetic waves by randomly distributed and oriented dielectric scatterers. *Phys. Rev. D*, **21**(2), 388–394, January 1980.

[33] N. Wellander and G. Kristensson. Homogenization of the Maxwell equations at fixed frequency. *SIAM J. Appl. Math.*, **64**(1), 170–195, 2003. doi: 10.1137/S0036139902403366.

[34] M. S. Wertheim. Exact solution of the Percus-Yevick integral equation for hard spheres. *Physical Review Letters*, **10**(8), 321–323, 1963.